Zeeman effect induced 0-π transitions in ballistic Dirac semimetal Josephson junctions

Supplementary information

Chuan Li[1], Bob de Ronde[1], Jorrit de Boer[1], Joost Ridderbos[1], Floris Zwanenburg[1], Yingkai Huang[2], Alexander Golubov[1,3], and Alexander Brinkman[1]

1 MESA +

Institute for Nanotechnology, University of Twente, The Netherlands

2 Van der Waals - Zeeman Institute, IoP, University of Amsterdam, The Netherlands

3 Moscow Institute of Physics and Technology, Dolgoprudny, Moscow Region, 14170, Russia

1. Theoretical model

To simulate the current-phase relation and it's temperature dependence in our measurement, we apply the formalism described on the basis of the Gor'kov equations [1][1], which are simplified by a quasi-classical approximation when the Fermi-wavelength is much smaller than other length scales in the system. For SNS Josephson junctions, Eilenberger quasi-classical equations are used when the elastic mean free path l_e is larger than the junction length L and the coherence length ξ, thus in the clean ballistic region. We have shown in our previous works, this is the case for the single crystalline $Bi_{1-x}Sb_x$ - based junctions.

Using Eilenberger equations, the supercurrent density J is expressed as [2]

$$J = \frac{2}{\pi} e k_F^2 k_B T \sin\chi \sum_{\omega_n>0} \int_0^1 \mu d\mu \frac{t_1(\mu) t_2(\mu)}{\frac{1}{Q^2}(\chi,\mu)} \qquad (1)$$

where $\mu = k_x/k_F$, $t_1, t_2 = \frac{D_{1,2}}{2-D_{1,2}}$, D_i is the transparency of each NS interface, and

$Q = \left[t_1 t_2 \cos\chi + \left(1 + (t_1 t_2 + 1)\frac{\omega_n^2}{\Delta^2}\right)\cosh\frac{2\omega_n L}{\mu\hbar v_F} + (t_1 + t_2)\frac{\omega_n \Omega_n}{\Delta^2}\sinh\frac{2\omega_n L}{\mu\hbar v_F}\right]^2 - (1 - t_1^2)(1 - t_2^2)\frac{\Omega_n^4}{\Delta^4}$, where $\omega_n = 2\pi k_B T(2n+1)$ is the Matsubara frequency, $\Omega_n = \sqrt{\omega_n^2 + \Delta^2}$. Δ is the gap in the S electrodes, χ is the phase difference across the junction and v_F is the Fermi velocity of the normal metal interlayer. The integral can take the full angle of the real sample geometry.

Here we employ a "planar SNS bridges" model to reflect on the practical fact that the area under the Nb leads are usually doped due to the band bending or etching induced defects and the proximized region of the N-film acts as an effective electrode with induced superconducting gap [3][4]. As stated in the main text, we first fit the overall temperature dependence ($I_c(T)$), then automatically one will get a current-phase relation for each temperature. The best fit gives a high transparency $D \sim 0.98$ with an induced superconducting gap $\Delta \approx 4.5K$(~0.7 meV).

According to our fitting results, the effective length $\bar{d} = \frac{L}{\xi}$ (where $\xi \equiv \frac{\hbar v_F}{2\pi k_B T_c}$ is the superconducting coherence length) can be obtained. If we take $T_c = 4.5K$, $v_F = 2.2 \times 10^5 m/s$, L = 200 nm, we get $\bar{d} = 2.53$. The total current $J_c = N.8.\frac{e}{\hbar} k_B T_c . \tilde{j}(T = 0)$. The numeric calculation gives a prefactor $\tilde{j}(T = 0) = 0.069$, and the current per mode is $8.\frac{e}{\hbar} k_B T_c . \tilde{j}(0)$=55nA/mode. Thus the estimated number of mode $N = \frac{J_c}{34nA} \approx 27$.

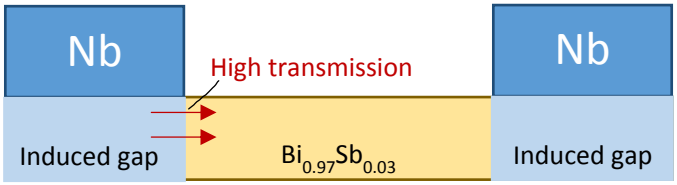

Figure s1 schematic draw of proximized Nb –$Bi_{1-x}Sb_x$- Nb junction. The high transmission is given by the doped region of $Bi_{1-x}Sb_x$ and the normal $Bi_{0.97}Sb_{0.03}$.

2. Sample fabrication and measurement setup

The Bi1-xSbx flakes are exfoliated with a scotch tape using similar techniques as for obtaining graphene. The good flakes are identified under optical microscope, then atomic force microscope (AFM). The contact structures are defined using a standard E-beam lithography, followed by a DC sputtering deposition of Niobium/Palladium (100nm/3nm) layers. The palladium layer is mainly for protecting the Nb from oxidation.

In Figure s2 we show the SEM photo of our sample. Most part of the SQUID is covered by a piece of unremoved Nb. 3 out of 6 samples resulted in a similar structure and performed as an effective SQUID. This “bad lift-off” process is mainly due to the charging effect near the contact on the substrate, where the isolating SiOx layer was charged easily with the same amount of writing current in e-beam lithography.

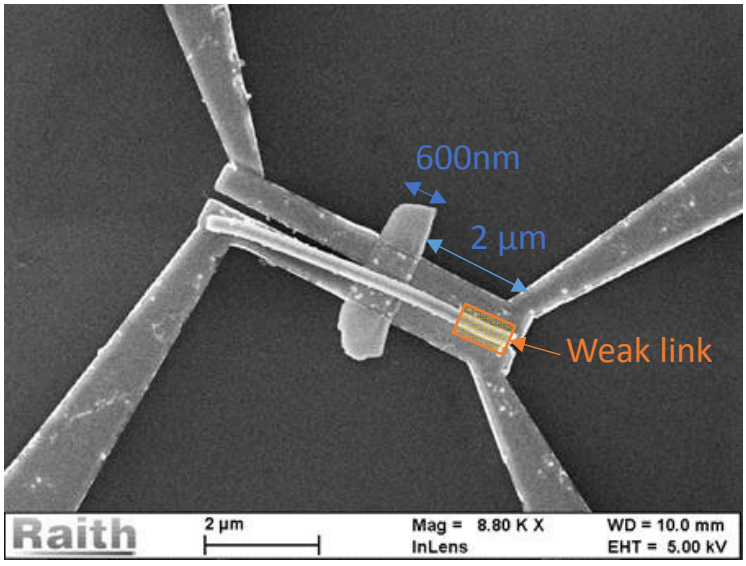

Figure s2- SEM photo of the sample. The Nb weak link formed by the unremoved piece of Nb (orange).

- SQUID period conversion

Based on the sample dimensions, the expected period of the current in magnetic field is given by $\Delta B = \frac{\phi_0}{s} \approx 3\ mT$, which is lightly larger than the actual measured period (2 mT, see the main text or *Figure s3*). We attribute this to the magnetic focusing effect, which gives roughly a 100 nm penetration length. Then the $\frac{\phi}{\phi_0}$ is directly converted from the measured the field value to the normalized value.

The measurement was carried out in a Triton-200 dry dilution fridge at the base temperature <30mK. All the results are obtained with a DC signal. At each field value, a I-V curve was obtained by sweeping the current. The I_c is then determined by setting a switching threshold. The I_s is extracted by subtracting the the averaged value from the measured Ic. Three-axis magnet is used in this experiment to apply magnetic field in different directions. A low-pass filter is installed in the dilution fridge.

3. In-plane vertical field dependence

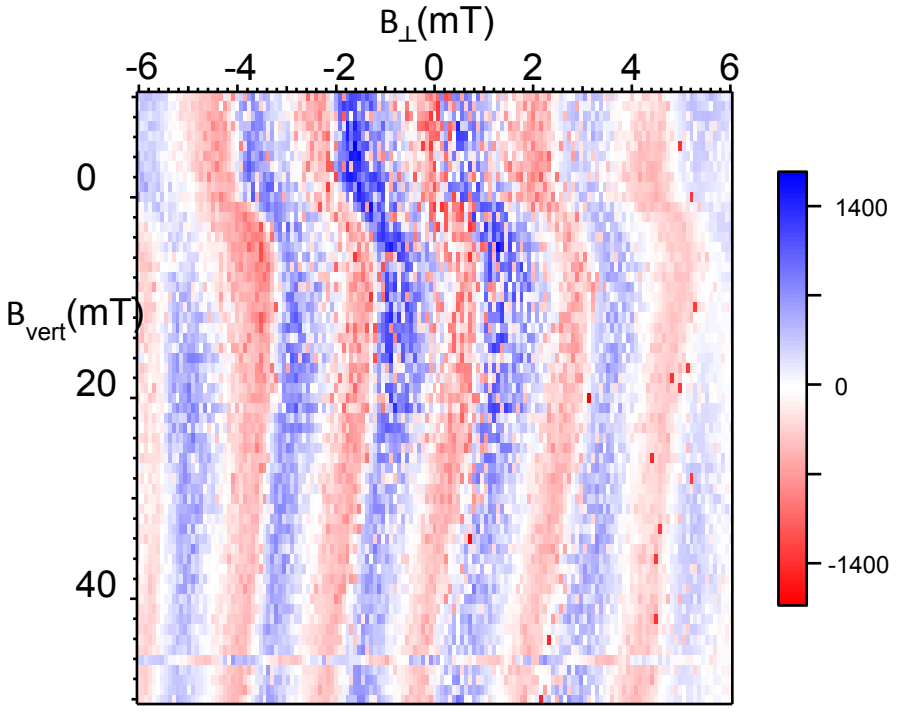

Figure s3 In-plane vertical field dependence.

We measured the CPR for an applied in-plane vertical magnetic field. The paramagnetic response of the superconducting leads is unstable near zero field, which can strongly perturb the phase-sensitive devices. After going through zero field, vortices can be randomly trapped in the environment, which shifts the original zero field to a finite value. At higher field, it becomes stable and the trapped vortices do not move.

4. Parallel field misalignment correction

A small misalignment can also induce a gradual phase shift in SQUID patterns. We show the simulated SQUID pattern with and without a tilting angle.

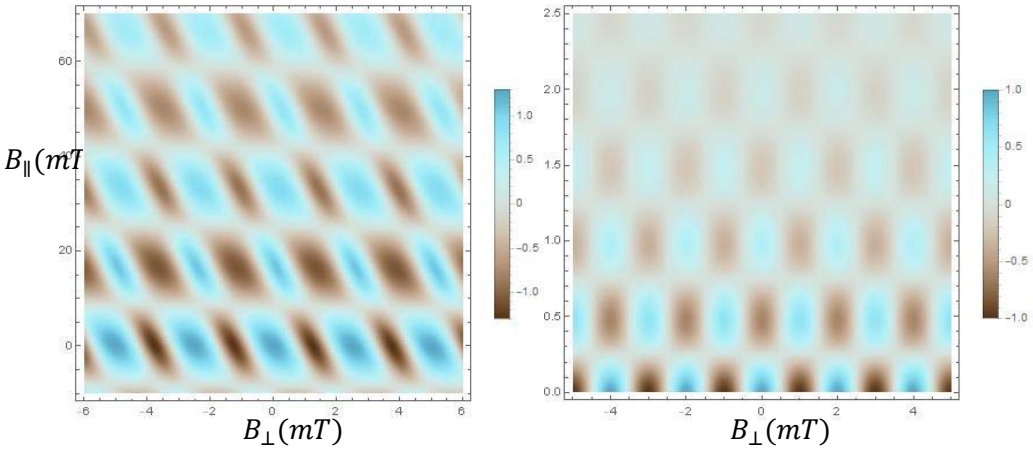

Figure 4 Simulation of SQUID patterns with and without tilting angle. Left: SQUID pattern with tilting angle $\theta = -4°$. Right: ideal SQUID pattern without tilting angle.

We simply introduce a small out-of-plane tilting angle θ, which results in a mixture of parallel field $B_{\parallel}$ and perpendicular field $B_{\perp}$:

$$B_{\parallel} = \sin\theta \cdot B_y + \cos\theta \cdot B_z$$

$$B_{\perp} = -\cos\theta \cdot B_y + \sin\theta \cdot B_z$$

The parallel field dependence of the critical current is given by

$$I_c^{para} = e^{-\beta|B_{\parallel}|\cdot\cos(2\pi B_{\parallel})}$$

and the total critical current is given by $I_c = I_c^{para}[I_s\cos(\pi B_{\perp}) - 0.2\cos(2\pi B_{\perp}) + 0.2]$, including the non-sinusoidal terms. We take $I_s = 1.3\mu A$, a parallel field decay of $\beta = 0.01T$ (as extracted from the fitting curve of main text), and $\theta = -4°$.

Reference

[1] Gor'kov, L.P. On the energy spectrum of superconductors. *Zh. Eksp. Teor. Fiz.* **34**, 735-739 (1958) [*Sov. Phys. JETP* **7**, 505-508 (1958)].

[2] Galaktionov, A.V. & Zaikin, A.D. Quantum interference and supercurrent in multiple-barrier proximity structures. *Phys. Rev. B* **65**, 184507 (2002).

[3] A.F.Volkov, P.H.C.Magnee, B.J.van Wees, T.M.Klapwijk, Proximity and Josephson effects in superconductor-two dimensional electron gas planar junctions, *Physica C* **242**, 261 (1995).

[4] G. Tkachov, Suppression of surface p-wave superconductivity in disordered topological insulators, *Phys. Rev. B* **87**, 245422 (2013).